

Nanostructured optical microchips for cancer biomarker detection

By: Tianhua Zhang, Yuan He, [Jianjun Wei](#), Long Que

T. H. Zhang; Y. He; J. Wei; L. Que, Nanostructured optical microchips for cancer biomarker detection, *Biosensors and Bioelectronics*, 2012, 38(1), 382-388.

***© Elsevier. Reprinted with permission. This version of the document is not the version of record. Figures and/or pictures may be missing from this format of the document. ***



This work is licensed under a [Creative Commons Attribution-NonCommercial-NoDerivatives 4.0 International License](#).

Made available courtesy of Elsevier: <https://doi.org/10.1016/j.bios.2012.06.029>

Abstract:

Herein we report the label-free detection of a cancer biomarker using newly developed arrayed nanostructured Fabry–Perot interferometer (FPI) microchips. Specifically, the prostate cancer biomarker free prostate-specific antigen (f-PSA) has been detected with a mouse anti-human PSA monoclonal antibody (mAb) as the receptor. Experiments found that the limit-of-detection of current nanostructured FPI microchip for f-PSA is about 10 pg/mL and the upper detection range for f-PSA can be dynamically changed by varying the amount of the PSA mAb immobilized on the sensing surface. The control experiments have also demonstrated that the immunoassay protocol used in the experiments shows excellent specificity and selectivity, suggesting the great potential to detect the cancer biomarkers at trace levels in complex biofluids. In addition, given its nature of low cost, simple-to-operation and batch fabrication capability, the arrayed nanostructured FPI microchip-based platform could provide an ideal technical tool for point-of-care diagnostics application and anticancer drug screen and discovery.

Keywords: Cancer biomarker detection | Arrayed nanostructured optical microdevices | Micromachined Fabry–Perot interferometer | Immunoassay

Article:

1. Background

The detection of cancers at their early stage is critical for the survival of the patients (Choi et al., 2010; Ferrari, 2005). In the field of genomics and proteomics, a variety of technologies have been developed for biomarker discovery and early detection, such as various DNA microarrays (Food et al., 1991), DNA sequence methods (Farwell and Joshi (2009)), enzyme-linked immunosorbent assay (ELISA) (Zangar et al., 2006), two-dimensional polyarylamide gel electrophoresis (2D-PAGE) (Choe et al., 2006), mass spectrometry (Ackermann et al., 2006), proteomic pattern diagnostics (Petricoin et al., 2004), and protein/antibody microarrays (Stoevesandt et al., 2009). However, most of them suffer from a complicated fluorescent dye labeling process, bulk instrumentation and low sensitivity, and are not applicable for trace

detection of biomarkers at the early stage of tumor diseases. For instance, sandwich ELISA is the gold standard in the detection and quantification of protein/cancer biomarkers (Imafuku et al., 2004). But sandwich assays are not convenient for achieving large scale multiplexed measurements (Lee et al., 2008). On the other hand, most fluorescence imaging based techniques are incapable of providing sufficient sensitivity to monitor biomarker affinity at concentrations of around 10 pM or lower without some forms of signal amplification (Healy et al., 2007). The concentration of many clinically relevant biomarkers residing in biofluids (i.e., blood) is usually at picomolar concentrations or lower (Lee et al., 2008), about five to seven orders of magnitude lower than the most abundant plasma protein. Since there is no universal ultrasensitive enzymatic amplification method for proteins like polymerase chain reaction (PCR) for the detection of nucleic acid, thus a diagnostic tool with ultrasensitivity (picomolar, femtomolar concentration or lower) and high specificity is required.

To this end, micro- and nano-technologies started to play a very important role in the enhancement of the sensitivity and detection limit of the biosensing technologies. A variety of different detection technologies based on micro- and nano-technologies have been developed in the past decades for the measurement of the tumor markers at a low concentration level, showing great promise for potential applications in point-of-care diagnostics and clinic settings. Representative technologies include fluorescence (Mukundan et al., 2009), light scattering (Liu et al., 2008), surface enhanced Raman spectroscopy (SERS) (Haynes et al., 2005), surface Plasmon resonance (SPR) (Smith and Corn, 2003), photonic crystals (Chan et al., 2008), electrochemical immunosensing electrodes (Wilson and Nie (2006)), quartz crystal microbalance (Henne et al., 2006), micro- or nano-cantilevers (Wu et al., 2000), nanowires (Zheng et al., 2005; Tian et al., 2011), carbon nanotubes (Star et al., 2006), nanoparticles based localized SPR (Nie and Emory (1997)), nanoholes and array (Yanik et al., 2005), quantum dots (Gao et al., 2004), magnetonanosensor (Gaster et al., 2009), nanopore thin film (Lin et al., 1997) technologies. Furthermore, recent technical advancement in nanofabrication, nanomaterial synthesis, micro/nanofluidics and bioassay has also enhanced the sensitivity or chip adaptability for the detection and quantification of protein biomarkers in biological samples via the binding to antibodies or aptamers (Zhou et al., 2007).

Among these technologies, particularly related to this article is the label-free optical detection technique. Label-free technique is attractive for biosensing since no fluorescent dyes are needed to be attached to the biomolecules. As a result, the experimental cost can be reduced dramatically, and the possible perturbation of the properties of the biomolecules can be totally avoided (Kingsmore, 2006). In terms of micro- and nano-technologies enabled optical techniques for label-free biodetection, the widely used ones include surface plasmon resonance (SPR), SERS, localized SPR, light scattering, photonic crystals, nanoholes, quantum dots, microspheres (Ren et al., 2007), opto-fluidic ring resonators (Gohring et al., 2010), microring resonators (Washburn et al., 2009), and thin film interferometric devices (Lin et al., 1997). These technologies can provide exceptional sensitivity and some of them can even offer detection limit down to the single molecule level, hence having great potentials for the early stage detection of cancer/disease biomarkers. Specifically, using these technologies, the detection of a variety of disease biomarkers such as carcinoembryonic antigen (CEA) for colon cancer, prostate-specific antigen (PSA) for prostate cancer, HER2 for breast cancer and amyloid-beta derived diffusible ligands (ADDLs) for Alzheimer disease has been demonstrated (Georganopoulou et al., 2005).

However, the aforementioned techniques still face some of the following issues: the complexity of the optical testing setup, expensive micro- or nano-fabrication process, or relative difficulty of miniaturization for fabricating integrated microchips. Recently, a class of inexpensive polymer-based nanostructured Fabry–Perot interferometer (FPI) optical microdevices has been developed (Zhang et al., 2010a, 2011). However, the anodic aluminum oxide (AAO) nanostructures inside the microdevices were fabricated from Al foil, which is not compatible with a standard lithography-based micro- or nano-fabrication process. As a result, it is impossible to fabricate arrayed nanostructured FPI optical devices in a cost-effective manner.

Herein, a new set of nanostructured FPI devices fabricated from the lithographically patterned AAO nanostructures on ITO glass substrates and its detection of prostate cancer biomarker free prostate-specific antigen (f-PSA) are reported for the *first* time. More specifically, compared to all other reported nanopore thin film based biosensors (Lin et al., 1997; Pacholski et al., 2006; Zhang et al., 2011), it is the first time to fabricate this type of arrayed sensors on a single chip, making the integration of arrayed sensors and microfluidic network much simple and cost-effective. PSA is a protein produced by cells of the prostate gland and has been used to detect prostate cancer at its early stage. Two forms of PSA, free or attached to a protein molecule, circulate in the blood. Usually a PSA level below 4.0 ng/mL is regarded as normal (Thompson et al., 2004). An elevated PSA level (>4 ng/mL) might be a sign of prostatitis, enlarged prostate or prostate cancer. Under benign prostate conditions, there is more f-PSA. Hence the lower the f-PSA in serum, the higher the possibilities of the prostate cancer. Fig. 1(a) illustrates the schematic and operational principle of the nanostructured Fabry–Perot interferometer (FPI) microchip. Inside the FPI cavity is a layer of nanopore structures coated with Au thin film. The optical transducing signal is the reflected optical interference signal from the nanostructured FPI microchip when a white light is incident normally on it. The close-up of the nanostructured FPI is shown in Fig. 1(b). When the biomolecules (e.g., antibody) are immobilized on the nanostructures and the binding between biomolecules (e.g., between antibody and biomarker) occur, the fringes of the reflected signals will shift due to the change of the effective refractive index inside the cavity. The nanostructure inside the FPI cavity increases the binding sites of the biomolecules thus the sensing surface area up to at least two orders of magnitude larger than that of a conventional FPI microdevice with a planar surface inside its cavity. In addition, the Au-coated nanostructure will enhance the transducing signals tremendously due to the localized surface Plasmon resonance effect. A photo of the fabricated 2×2 nanostructured FPI chips is shown in Fig. 1(c).

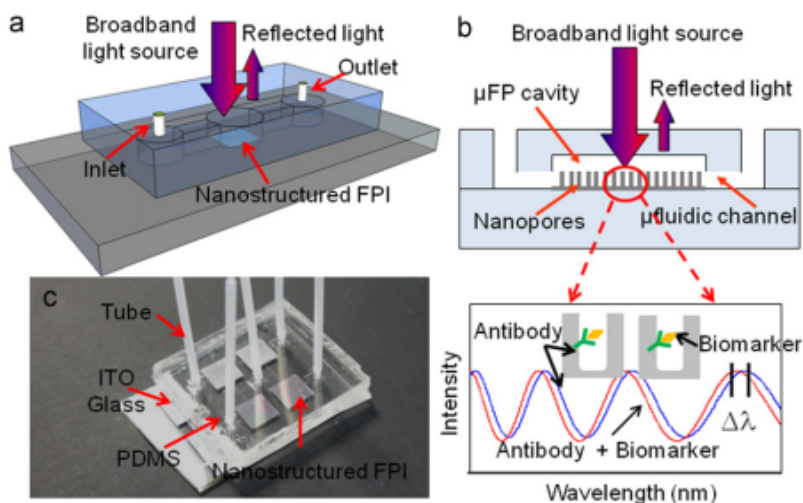


Fig. 1. (a) Schematic of a 3-D nanostructured FPI device; (b) Close up showing the nanostructures (i.e., nanopores) inside the cavity of a nanostructured FPI device: the immobilization of biomolecules (i.e., antibody) on the surface of the nanostructures and the binding between biomolecules (i.e., antibody and biomarker) will change the effective index of refraction and thus effective optical thickness, causing the shift of the reflected interference fringes. (c) Photo of a fabricated 2×2 nanostructured FPI devices with assembled microfluidic interface.

2. Methods and materials

2.1. Fabrication of nanostructured optical device and microfluidic interface assembly

The fabrication process flow is illustrated in Fig. 2. Briefly, this process starts from an ITO glass substrate. A lift-off process is used to form the Al patterns. As a result, Al patterns are formed and connected with each other with Al lines as shown in Fig. 2(b). Once the Al patterns have been fabricated and cleaned with acetone and DI water, two-step anodization using oxalic acid has been carried out to form AAO nanostructures as shown in Fig. 2(c). Then a layer of Au thin film (10, 15 and 50 Å) was coated on AAO with a layer of Cr (5 Å) as an adhesion layer. A polydimethylsiloxane (PDMS) microfluidic chip was fabricated separately using a soft lithography process described in Fig. 2(e) and then was bonded with the AAO-glass chip followed by assembling input and output tubing as shown in Fig. 2(f). The input tube was connected with a syringe controlled by a syringe pump while the output tube led to a biochemical waste collecting beaker. It should be noted that the Au-coated AAO patterns were totally inside the FPI cavity as shown in Fig. 1(c) in order to ensure that the PDMS microfluidic layer was directly bonded to the glass, thus avoiding any liquid leakage during the operation of the nanostructured FPI microchip. The SEM images of the fabricated AAO are shown in Fig. 2(g–h). The detailed fabrication process of the arrayed nanostructured FPI devices can be found in supplementary material.

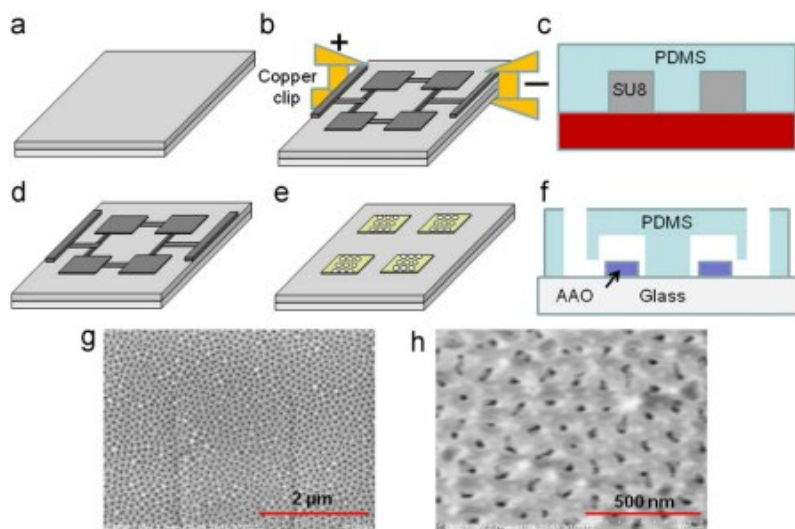


Fig. 2. (a–f) Fabrication process flow of the 2×2 nanostructured FPI devices from ITO glass substrate, which can be readily modified to fabricate large-scale arrayed nanostructured FPI devices; (g–h) SEM images of AAO nanostructures.

Three sets of nanostructured FPI microchips have been fabricated and each microchip has four identical devices as shown in Fig. 1(c) for the following experiments: (i) **Set I**: monitoring of the self-assembled monolayer (SAM) formation and upper detection range measurement; (ii) **Set II**: determination of the limit-of-detection, and (iii) **Set III**: control experiments on specificity and selectivity of the bioassay. The nanopore size is the same for all microdevices in the three sets, but the thickness of Au thin film is different, which gives essentially the similar optical performance (i.e., optical contrast), even though the transducing signals (i.e, positions of the fringe peaks) from the nanostructured FPI microdevices have some difference (Zhang et al., 2010a).

2.2. Instrumentation

A broadband light source from a tungsten halogen lamp with spectrum covering 350–1050 nm is coupled to a specifically designed optical fiber probe (Ocean Optics, Inc), which illuminates the microchip perpendicularly as shown in Fig. 1(a–b) (Zhang et al., 2010b). The reflected signals (transducing signals) are collected by the same optical fiber probe, leading to an optical spectrometer (Ocean Optics, Inc), which is connected to a laptop computer for data acquisition and processing. The biochemical samples are transported to the microdevice through the assembled plastic tubing (Upchurch Scientific, Inc.) by a syringe controlled by a syringe pump (KD Scientific, Inc.).

2.3. Chemicals and materials

11-Mercaptoundecanoic acid ($\text{HSC}_{10}\text{COOH}$, 99%), 8-Mercapto-1-Octanol (HSC_8OH , 98%), N-(3-Dimethylaminopropyl)-N'-ethylcarbodiimide hydrochloride (EDC), N-Hydroxysuccinimide (NHS), and glycine were purchased from Sigma-Aldrich (Milwaukee, WI) and used without further purification. Mouse anti-human prostate-specific antigen (PSA) monoclonal antibody (detector mAb) (cat.# T40081B, clone # CHYH2), ELISA kits for human free-PSA (Cat.# 10050) were obtained from Anogen-YES Biotech Laboratories Ltd. (Mississauga, Canada). The 10 ng/mL free-PSA standard solution was used for preparation of free-PSA solutions with lower

concentrations using sample dilutant provided in the ELISA kit. The 10 ng/mL free-PSA standard solution was prepared in a protein matrix solution according to the WHO standard by the vendor. The concentrations of diluted free-PSA include 0, 5, 10, 50, 100, 500, 5000 pg/mL for the experiments. Absolute ethanol was obtained from Thermo Fisher Scientific Inc., USA. Dionized (DI) water was obtained from a DI water purification system (Millipore, FRANCE). Bovine serum albumin (BSA) was obtained from Bio-Rad Laboratories, USA. It was diluted with PBS (pH=7.2) solution at several different concentrations of 50, 100, 500, 5000 pg/mL for the control experiments. Rabbit Immunoglobulin G (Rabbit-IgG) was purchased from Sigma-Aldrich and was diluted using PBS (pH=7.2) solution to several different concentrations of 50, 100, 500, 5000 pg/mL for the control experiments.

2.4. Biodetection procedures

2.4.1. Immobilization of detector mAb on the gold surface

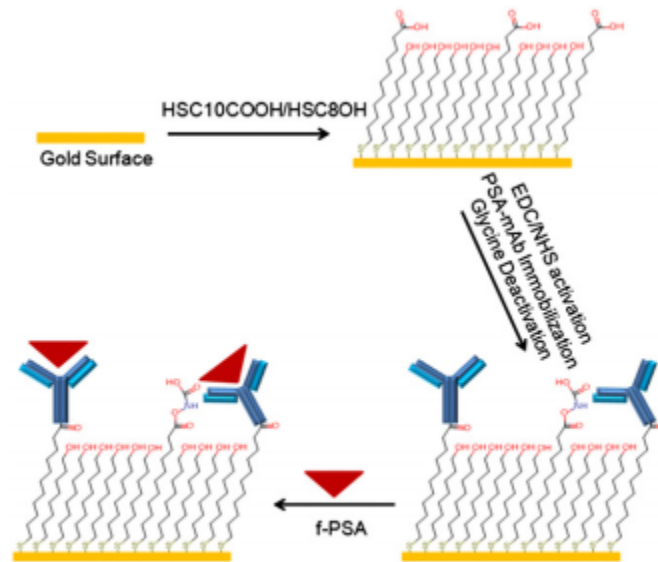


Fig. 3. Illustration of the protocol for the self-assembled monolayer (SAM) formation on the Au-coated nanostructures, antibody (mAb) immobilization and f-PSA testing.

2.4.2. f-PSA detection

Once the antibodies (mAbs) have been immobilized on the gold-coated nanostructured surface in the microchip, the detection of f-PSA was ready as shown in Fig. 3. The f-PSA is the unbounded form of the antigen and normally at the level of 10% of total PSA. A higher amount of f-PSA in a test means a lower chance of cancer. During the experiments, PBS was used as a running buffer to help minimize or avoid the nonspecific adsorption of the f-PSA in the tubes and the microfluidic channels.

2.4.3. Control experiment

Two types of control experiments have been designed and carried out to evaluate the specificity/selectivity of the immunoassay using the nanostructured FPI microdevices.

Specifically, the binding between the detector mAb and BSA at concentrations of 50, 100, 500, 5000 pg/mL has been evaluated, respectively. In addition, the binding between the detector mAb and rabbit IgG at several different concentrations has also been evaluated.

2.5. Experimental data analysis

The average shift of the fringes for the measured transducing signals is obtained by (i) first obtaining the shift of each fringe peak relative to that of the blank Au-coated nanostructure surface or that after the antibodies (mAbs) have been immobilized on the nanostructure surface, then (ii) averaging the shift of all the peaks. The reference for each average shift is specified in the context in the following sections.

The effective optical thickness (EOT) of the nanostructure layer and the biomolecules immobilized on it is obtained by performing Fourier transform on the measured optical transducing signals, which were described in detail in the citation (Zhang et al., 2010a). A MATLAB program based on the fast Fourier transform algorithm has been developed for this calculation.

3. Results and discussion

3.1. Surface functionalization of the Au-coated nanostructures

The surface functionalization of the Au-coated nanostructures was performed step by step following the protocol illustrated in Fig. 3. It is a well-established method to form a mixed SAM of alkanethiols by the adhesion reaction of the thiol group on gold surface (Cass and Ligler, 1998). The monolayer is well packed and the tethered carboxylic acid is easy to be functionalized for biological molecule immobilization (Wei et al., 2004). Upon the presence of EDC/NHS, the carboxylic groups form active O-acylisourea intermediates, and readily react with primary amine groups which exist at the N-terminus of each polypeptide chain and in the side chain of lysine (Lys, K) residues. Because of their positive charge at physiologic conditions, primary amines are usually outward-facing (i.e., on the outer surface) of proteins; hence, they are usually accessible for conjugation without denaturing protein structure. In such a way, the detector mAbs for f-PSA are covalently attached to the top of the mixed SAMs. The remaining active O-acylisourea intermediate groups are deactivated by the amino acid glycine to avoid non-specific biological attachment caused by the intermediates. At this stage, the mAbs are conjugated to the nanostructured surface and ready for f-PSA detection.

Since each aforementioned surface chemical modification step changes the local refractive index and the effective optical thickness of the nanostructured surface, hence each step can be monitored optically in real time. The real-time monitoring experiments have been carried out on four individual nanostructured FPI microchips in the **Set I**, giving consistent results. As an example, Fig. 4(a) gives a representative step-by-step measurement during the surface functionalization. As we can see, the interference fringes (transducing signals) shift clearly after each step of addition of organic molecules and biomolecules. It should be noted that all these measurements were performed at room temperature. The measured interference fringes for the antibody attachment were obtained after totally 2-hour incubation and three cycles of rigorous

PBS solution rinsing. Compared to the fringes obtained on the nanostructured FPI microchip with a blank gold-coated nanostructured surface in the range of 550–850 nm, typical average shift was 5.13 ± 0.02 nm after the HSC10COOH/HSC8OH was added and reacted with the gold-coated surface, 9.48 ± 0.02 nm after EDC/NHS was added and reacted with the surface, 13.68 ± 0.02 nm after the antibodies (mAbs) were added and attached to the surface.

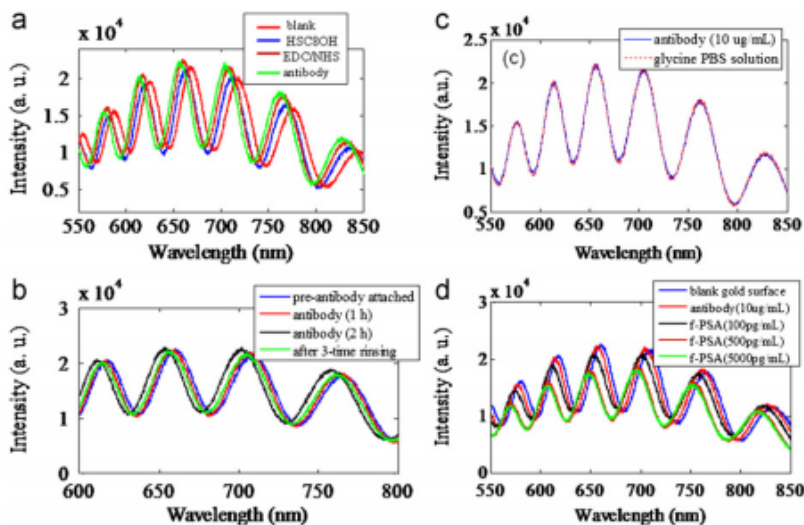


Fig. 4. (a) Measured transducing signals showing the step-by-step formation of SAM and immobilization of antibodies (mAbs) using the microdevices in **Set I**; (b) Measured transducing signals showing the process for the attachment of antibodies (mAbs); (c) Measured transducing signals before and after glycine PBS solution is applied to avoid non-specific binding; (d) Upper detection range for a device with limited amount of immobilized antibodies (mAbs) on the device in **Set I**: by increasing the concentration of f-PSA, eventually no shift in the transducing signals was observed, indicating all the binding sites for f-PSA have been occupied.

The more detailed real-time monitoring of the process of the attachment of antibodies (mAbs) is given in Fig. 4(b). When the mAbs were flowed into the chip, the optical signals were monitored at different time interval. As we know that it would take some time for antibodies to be immobilized and attached to the SAM layer. The measurements showed clearly the shift of the fringes after 1-hour incubation at room temperature relative to that of pre-antibody being applied. The shift further increased after 2-hour incubation, indicating that possibly more antibodies had been immobilized or attached. Thereafter, three-time rigorous rinsing by flowing PBS solution was carried out to remove the unbounded or loosely bounded antibodies. As expected, the shift of the fringes decreased relative to that of pre-antibody attached condition, namely the fringes had a red-shift. Experiments found that after 3 cycles of rinsing using PBS solution, no further shift of the fringes was observed, suggesting that all the unbounded antibodies had been got rid of from the microchip. Compared to the fringes of pre-attachment of the antibodies, the measured final average fringe shift was 4.21 ± 0.02 nm after antibodies were attached and immobilized. Thereafter, a glycine PBS solution is applied to avoid non-specific binding between SAM and f-PSA, negligible shift of the fringes has been observed as shown in Fig. 4(c), indicating that the active sites at SAM have been totally or almost totally occupied by mAbs, and thus no or very few amino acid glycine is attached to them.

The real-time monitoring of the transducing signals is an important step to verify that each chemical modification of the sensing surface has actually occurred. This measurement is particularly useful and effective since we do not need utilize any fluorescent dyes to tag the organic molecules or biomolecules to visually observe and thus confirm the occurrence of each

surface modification. In addition, it is also a simple approach to ensure that the unbounded and loosely bounded molecules have been totally rinsed away. This is a critical step to warrant the consistent measurements from each microchip, especially for future reliable and reproducible arrayed microchips for multiplexed biodetection.

3.2. Detection of cancer biomarker free-PSA

After the antibodies (mAbs) are immobilized on the Au-coated nanostructured surface inside the microchip, the quantitative measurement of f-PSA can be carried out.

3.2.1. Upper detection range

The effect of the amount of the antibodies immobilized on the microchips on the upper detection range of the f-PSA has been evaluated. In this set of experiments, the antibody (mAb) concentration was 10 $\mu\text{g}/\text{mL}$ and the incubation time was 2 h. The concentrations of f-PSA flowed into the microchip were 100, 500 and 5000 pg/mL in a PBS solution. The order of the experiments was designed as the following. The f-PSA was flowed into microchip from lower concentration to higher concentration sequentially. For instance, the f-PSA at concentration of 100 pg/mL was flowed into the chip first, after 45 min incubation, PBS solution was flowed to rinse the microchip three times and measurements were carried out accordingly. Then the f-PSA at higher concentrations (i.e., 500 and 5000 pg/mL) were flowed into the chip. After incubation, a rinsing and measurement routine was carried out again. It was found that the binding sites had been almost totally occupied after f-PSA at concentration of 500 pg/mL was flowed into the chip since the interference fringes remained essentially unchanged even more f-PSA was added. As an example, the measurement in Fig. 4(d) shows that when the concentration of f-PSA reached 5000 pg/mL , there was little observable shift of the fringes compared to that of f-PSA at a concentration of 500 pg/mL , indicating the upper detection range of f-PSA was about 500 pg/mL . If we want to expand the upper detection range, basically we have to immobilize more antibodies on the microchip so that more binding sites are available for f-PSA. However, it should be also noted that the amount of the antibodies cannot be too excessive; otherwise the antibodies immobilized on the sensing surface are too closely packed and crowded to allow f-PSA to approach the binding sites efficiently and consequently to be attached to them. For instance, in one of our experiments, antibodies (mAbs) at a concentration of 100 $\mu\text{g}/\text{mL}$ were immobilized on the sensing surface with 24-hour incubation, the f-PSA at several concentrations was flowed into the chip for the testing. After rinsing by the PBS solution, it turned out that essentially no f-PSA had been attached to the antibodies, resulting in negligible shift in the fringes.

3.2.2. Limit of detection (LOD)

The experiments were carried out on four individual microchips in **Set II**. All the measurements gave consistent results. In this case, the antibodies at a concentration of 10 $\mu\text{g}/\text{mL}$ were flowed into the chip with incubation time of 4 h. The concentrations of f-PSA flowed into the microchip were 0, 5, 10, 50, 100 and 500 pg/mL in a PBS solution. The f-PSA was flowed into microchip from lower concentration to higher concentration sequentially. Specifically, the f-PSA at concentration of 0 pg/mL was flowed into the chip first, after sufficient time (45 min) for

incubation, the PBS solution was flowed to rinse the microchip three times and measurements were carried out. Thereafter, the f-PSA at concentration of 5 pg/mL was flowed into the microchip for the testing. After 45-minute incubation, a rinsing and measurement routine was carried out. Similarly, the experiments were performed for f-PSA at concentrations of 10, 50, 100, and 500 pg/mL in sequence, respectively. All these results were obtained by multiple measurements on four individual microchips, and the average fringe shift for each concentration was obtained accordingly.

Fig. 5(a–b) shows a representative measurement of the transducing signals with the f-PSA flowed into microchip at concentrations of 0, 5, 10, and 100 pg/mL. As expected, the interference fringes showed no or negligible shift with the f-PSA at 0 pg/mL since no f-PSA was actually available to be bounded to the antibodies. The average shift of the fringes was about 2.19 ± 0.02 nm with the f-PSA at a concentration of 5 pg/mL in the range of 550–850 nm, relative to the fringes for the device with immobilized antibodies. By increasing the concentration of the f-PSA to 10, 50, 100, and 500 pg/mL in sequence, the average fringe shift increased as expected since increasing amount of f-PSA were bounded to the antibodies. Experiments have also found that the fringe shift was not clearly distinguishable when the concentration of the f-PSA was below 5 pg/mL using these microchips for the experiments. This might be due to the resolution limit (± 0.02 nm) of the optical spectrometer used in the experiments or the detection limit of these microchips, indicating that the lowest detectable concentration of f-PSA by current microchips is about 5 pg/mL.

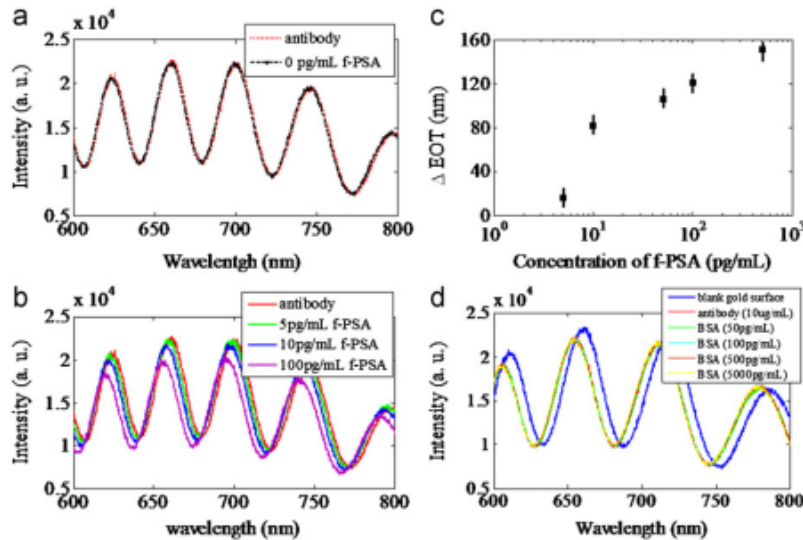


Fig. 5. Measured transducing signals with different concentrations of f-PSA using microdevices in **Set II**: (a) 0 pg/mL and (b) 5, 10, 100 pg/mL; (b) The change of the effect optical thickness (Δ EOT) with different concentrations of the f-PSA from 0, 5, 10, 50, 100, to 500 pg/mL based on the measurements on the microdevices in **Set II**. The error bars are the standard deviation of the values determined from measurements on four microdevices; (d) Controlled experiment using microdevices in **Set III**: no shift in fringes is observed, indicating that there is no binding between the antibodies (mAbs) and BSA.

Fourier transform has been applied on the measured transducing signals, and the effect optical thickness (EOT) of the nanostructured layer and the biomolecules immobilized on it has been obtained. Using the EOT after the immobilization of the antibodies as a reference, which is 7487 ± 2 nm, the change of the EOT (Δ EOT) after applying f-PSA at different concentrations has been obtained. In Fig. 5(c), the change of the effective optical thickness (Δ EOT) under different concentrations of the f-PSA is summarized. As expected, the lower concentration of the f-PSA,

the less the f-PSA was bounded to the antibodies, hence the smaller the Δ EOT. The EOT for each case was obtained by averaging several measurements. As can be seen, the Δ EOT has a linear dynamic range with the concentration of f-PSA from 10 to 500 pg/mL. However, at 5 pg/mL of f-PSA, the lowest detectable concentration, its Δ EOT has a relatively big change and deviated from the linear relationship, which might be related to the experiment procedure performed by increasing the concentration of the f-PSA. Hence, at current stage and for safety, the limit-of-detection (LOD) of the sensor is about 10 pg/mL or lower, which is \sim 280 fM, for the detection of f-PSA.

Finally, the control experiments have been carried out on the microchips in the **Set III** to demonstrate the specificity and selectivity of the bioassay. In this case, the incubation time of antibodies at a concentration of 10 μ g/mL was 4 h. The BSA solutions with different concentrations of 50, 100, 500 and 5000 pg/mL have been flowed into the microdevice sequentially. For each concentration of BSA, the incubation time was 60 min, followed by rigorous PBS solution rinsing three times. Representative measurements are given in Fig. 5(d). No or negligible shift in fringes has been observed when the BSA with four different concentrations was applied to the microchips, confirming the specific recognition between the antibodies (mAbs) and the f-PSA. Similarly, we performed experiments to check if the antibodies were bounded to rabbit IgG at concentrations of 50, 100, 500 and 5000 pg/mL, respectively. No or negligible shift in the fringes has been observed, indicating again that the antibodies were only specific to the f-PSA. Overall, these two types of control experiments (BSA and rabbit IgG) suggest the excellent selectivity of the immunoassay.

It should be noted that even though the three sets of devices have somewhat different transducing signals (i.e. the positions of the fringe peaks were different), for each set of the devices, a nanostructured FPI microchip with a blank gold-coated nanostructured surface from the same set was used as the reference, hence consistent measurement results for the bioassay have been obtained for the aforementioned three types of tests. In addition, it should be noted that the incubation time for the antibodies is unnecessary to be 2 or 4 h as confirmed by the experimental results in Fig. 4(b). In contrast, about 1.5-hour incubation time for the antibodies is sufficient. Actually with 2-hour or 4-hour incubation, significant amount of the antibodies is still unbounded due to no more available binding sites and will be removed by PBS solution rinsing.

As demonstrated, the nanostructured FPI microchips can offer sufficient sensitivity for the detection of clinically relevant cancer biomarkers, which are typically in the range of picomolar concentration level or lower. Furthermore, even though this paper only reports the detection of one cancer biomarker, since arrayed microchips can be batch-fabricated in an inexpensive and efficient manner, a disposable platform based on arrayed nanostructured FPI microchips can be developed for the multiplexed biomolecular detection and analysis in the future.

4. Conclusions

In summary, the detection of f-PSA has been demonstrated using nanostructured FPI microchips successfully. It has been demonstrated that the chemical and biochemical functionalization of the nanostructured sensing surface can be monitored in real-time. The upper dynamic detection range can be changed by varying the amount of capture antibodies immobilized on the sensing

surface. Currently the limit-of-detection (LOD) of the nanostructured FPI microchip for f-PSA is about 10 pg/mL or lower, which could be further lowered down by optimizing the optical properties (e.g., finesse) of the microchips. Experiments have also demonstrated the high specificity and selectivity of the immunoassay used in the biosensing, indicating the great promise for the detection of cancer biomarkers at trace levels in biofluids. Finally, due to the feasibility of fabricating hundreds of nanostructured FPI microdevices on a single chip, this technical platform offers great potential for highly multiplexed, label-free biodetection for the diagnosis of various cancers or diseases in a clinic setting and for anticancer drug screen and discovery applications.

Acknowledgments

The research is funded in part by NSF CAREER Award ECCS0845370 and NSF-Pfund 2009.

References

- Ackermann, B., Hale, J., Duffin, K., 2006. *Current Drug Metabolism* 7, 525–539.
- Cass, T., Ligler, F., 1998. *Immobilized Biomolecules in Analysis: A Practical Approach*. Oxford University Press, UK.
- Chan, L., Gosangari, S., Watkin, K., Cunningham, B.T., 2008. *Sensors and Actuators B* 132, 418–425.
- Choe, L., Werner, B., Lee, K., 2006. *NeuroRx : The Journal of the American Society for Experimental NeuroTherapeutics* 3, 327–335.
- Choi, Y., Kwak, J., Park, J., 2010. *Sensors* 10, 428–455.
- Farwell, L., Joshi, V., 2009. *Methods in Molecular Biology (Clifton, NJ)* 520, 205–220.
- Ferrari, M., 2005. *Nature Reviews Cancer* 5, 161–171.
- Food, S., Pirrung, M., Stryer, L., Lu, A., Solas, D., 1991. *Science (New York, NY)* 251, 767–773.
- Gao, X., Cui, Y., Levenson, R., Chung, L., Nie, S., 2004. *Nature Biotechnology* 22, 969–976.
- Gaster, R., Hall, D., Nielsen, C., Osterfeld, S., Yu, H., Mach, K., Wilson, R., Murmann, B., Liao, J., Gambhir, S., Wang, S., 2009. *Nature Medicine* 15, 1327–1332.
- Georganopoulou, D., Chang, L., Nam, J., Thaxton, C., Mufson, E., Klein, W., Mirkin, C., 2005. *Proceedings of the National Academy of Sciences of the United States of America* 102 (7), 2273–2276.

- Gohring, J., Dale, P., Fan, X., 2010. *Sensors and Actuators B* 146, 226–230. Haynes, C., McFarland, A., Van Duyne, R., 2005. *Analytical Chemistry*, 338–346.
- Healy, D., Hayes, C., Leonard, P., McKenna, L., O’Kennedy, R., 2007. *Trends in Biotechnology* 25, 125–131.
- Henne, W., Doorneweerd, D., Lee, J., Low, P., Savran, C., 2006. *Analytical Chemistry* 78 (14), 4880–4884.
- Imafuku, Y., Omenn, G., Hanash, S., 2004. *Disease Markers* 20, 149–153. Kingsmore, S., 2006. *Nature Reviews Drug Discovery*, 1–11.
- Lee, H., Wark, A., Corn, R.M., 2008. *Analyst* 133 (8), 975–983.
- Lin, V., Motesharei, K., Dancil, K., Sailor, M., Ghadiri, M., 1997. *Science (New York, NY)* 278, 840–843.
- Liu, X., Dai, Q., Austin, L., Coutts, J., Knowles, G., Zou, J., Chen, H., Huo, Q., 2008. *Journal of the American Chemical Society* 130, 2780–2782.
- Mukundan, H., Xie, H., Anderson, A., Grace, W., Shively, J., Swanson, B., 2009. *Bioconjugate Chemistry* 20 (2), 222–230.
- Nie, S., Emory, S., 1997. *Science (New York, NY)* 275, 1102–1106.
- Pacholski, C., Yu, C., Miskelly, G.M., Godin, D., Sailor, M.J., 2006. *Journal of the American Chemical Society* 128, 4250–4252.
- Petricoin, E., Rajapaske, V., Herman, E., Arekani, A., Ross, S., Johann, D., Knapton, A., Zhang, J., Hitt, B., Conrads, T., Veenstra, T., Liotta, L., Sistiare, F., 2004. *Toxicologic Pathology* 32 (Suppl 1), 122–130.
- Ren, H., Vollmer, F., Arnold, S., Libchaber, A., 2007. *Optics Express* 15, 17410–17423.
- Smith, E., Corn, R., 2003. *Applied Spectroscopy* 57 (11), 320A–332A.
- Star, A., Tu, E., Niemann, J., Gabriel, J., Joiner, C., Valcke, C., 2006. *Proceedings of the National Academy of Sciences of the United States of America* 103 (4), 921–926.
- Stoevesandt, O., Taussig, M., He, M., 2009. *Expert Review of Proteomics* 6 (2), 145–157.
- Thompson, I., Pauler, D., Goodman, P., et al., 2004. *New England Journal of Medicine* 350 (22), 2239–2246.
- Tian, R., Regonda, S., Gao, J., Lin, Y., Hu, W., 2011. *Lab on a Chip* 11, 1952–1961. Washburn, A., Gunn, L., Bailey, R.C., 2009. *Analytical Chemistry* 81 (22), 9499–9506.

Wei, J., Liu, Y., Niki, K., Margoliash, E., Waldeck, D., 2004. *Journal of Physical Chemistry B* 108, 16912–16917.

Wilson, B., Nie, W., 2006. *Analytical Chemistry* 78, 6476–6483.

Wu, G., Datar, R., Hansen, K., Thundat, T., Cote, R., Majumdar, A., 2000. *Nature Biotechnology* 19, 856–860.

Yanik, A., Cetin, A., Huang, M., Artar, A., Mousavi, S., Khanikaev, A., Connor, J., Shvets, G., Altug, H., 2005. *Proceedings of the National Academy of Sciences of the United States of America* 108 (29), 11784–11789.

Zangar, R., Daly, D., White, A., 2006. *Expert Review of Proteomics* 3, 37–44.

Zhang, T., Gong, Z., Giorno, R., Que, L., 2010a. *Optics Express* 18 (19), 20282–20288. Zhang, T., Pathak, P., Karandikar, S., Giorno, R., Que, L., 2011. *Biosensors and Bioelectronics* 30, 128–132.

Zhang, T., Talla, S., Gong, Z., Karandikar, S., Giorno, R., Que, L., 2010b. *Optics Express* 18 (17), 18394–18400.

Zheng, G., Patolsky, F., Cui, Y., Wang, W., Lieber, C.M., 2005. *Nature Biotechnology* 23 (10), 1294–1301.

Zhou, L., Ou, L., Chu, X., Shen, G., Yu, R., 2007. *Analytical Chemistry* 79 (19), 7492–7500.